Available online at www.sciencedirect.com
SCIENCE DIRECT
Journal of Marine Systems 60 (2006) 345–364
JOURNAL OF MARINE SYSTEMS
www.elsevier.com/locate/jmarsys

Phytoplankton size classes competitions at sub-mesoscale in a frontal oceanic region

Pascal Rivière *, Philippe Pondaven

Laboratoire des Sciences de l'Environnement Marin, UMR 6539 UBO-CNRS, Institut Universitaire Européen de la Mer, Place Nicolas Copernic, 29280 Plouzané, France

Received 26 May 2005; received in revised form 31 January 2006; accepted 1 February 2006
Available online 4 April 2006

Abstract

The effects of mesoscale and sub-mesoscale dynamics on the competition between two different phytoplankton size classes are investigated with a 3D primitive equations model. The model reproduces realistic simulations of mesoscale turbulence generated by a westward current in the southern hemisphere at statistical equilibrium in a summer situation. Effects of two different grazing pressures on phytoplankton competitions are compared and the role of eddy variability is quantified comparing high and low resolution simulations.

High resolution simulations reveal a filamentary distribution of biomass and nutrients induced by the combination of vertical advection and horizontal stirring. This fine scale variability is observed not only on the horizontal but also on the vertical into the subsurface chlorophyll maximum.

One of the key results is that such a dynamics induces a spatial segregation of the phytoplankton in the southern part of the frontal region that is mainly filamentary. This spatial segregation consists in biomass maxima for large phytoplankton in rich nutrients filaments and maxima for small phytoplankton outside these filaments. This anti-correlation is particularly strong when grazing pressure is low and is confirmed by statistical analysis. In the central frontal region, dominated by mesoscale dynamics, the two phytoplankton classes are strongly correlated together and biomass maxima are located close to downwelling regions that are poor in nutrients.

It is shown that the effect of grazing is significantly amplified by the fine scale dynamics and that the combination of these two mechanisms is responsible of a switch of the ecosystem dominance in the surface layers.

In addition, the effect of frontal dynamics on the detritus export is very sensitive to grazing pressure: increasing grazing induces a significant decrease of the export in the presence of frontal dynamics whereas it induces an increase of the export without small-scale variability.

1. Introduction

In the ocean, bottom-up control of primary production is driven by the relative availability of light and of potential limiting nutrients. Light and nutrients are usually vertically separated because of biological uptake of nutrients within the surface layers, and subsequent export and remineralization of organic matter into the deep aphotic ocean. In the absence of terrestrial or atmospheric inputs of nutrients, stimulation of primary production thus requires nutrients inputs from the aphotic zone. It has been increasingly recognized that vertical motions associated with unstable fronts and

* Corresponding author. Tel.: +33 2 98 49 86 59; fax: +33 2 98 49 86 45.
E-mail address: Pascal.Riviere@univ-brest.fr (P. Rivière).

0924-7963/$ - see front matter © 2006 Elsevier B.V. All rights reserved.
doi:10.1016/j.jmarsys.2006.02.005

eddies are key mechanisms by which nutrients are injected into the euphotic zone. Indeed both observations and models show that fronts and mesoscale structures are usually characterized by higher primary production rates and higher plankton biomass compared to adjacent waters, especially in oligotrophic environments (Falkowski et al., 1991a,b; Flierl and Davis, 1993; Dadou et al., 1996; McGillicudy and Robinson, 1997; Oschlies and Garçon, 1998; Spall and Richards, 2000; Mahadevan and Archer, 2000; Martin et al., 2001; Lévy et al., 2001). In these regions a high spatial and temporal variability of biological response is observed.

Recent developments of modeling studies have greatly improved our understanding of the mechanisms by which this heterogeneity is generated. Abraham (1998) has shown that horizontal advection associated with mesoscale structures can induce small-scale plankton patchiness by stirring of spatial gradients. In addition, it has been shown that the combination of vertical advection and diffusion of nutrients into the euphotic zone can strongly stimulate local primary production (Lévy et al., 2001). And lastly the phase relationship between horizontal and vertical velocities has also a significant effect on primary production (Martin et al., 2002). This latter effect is expected to be more efficient into filamentary regions. These different mechanisms constrain strongly the surface primary production but also the deep chlorophyll maximum (DCM) usually observed in these frontal regions (Hood et al., 1991; Claustre et al., 1994; Hitchcock et al., 1993). In particular it has been shown that the nutrient enrichment mechanisms, the low grazing pressure at these depths and the sinking of phytoplankton cells play a major role in the formation of the DCM (Claustre et al., 1994, Franks and Walstad, 1997, Lévy et al., 2001).

Most of the recent modeling studies on physical–biological interactions at sub-mesoscale used classical simple ecosystem models as *N–P–Z–D*, and less attention has been given to the role of functional diversity in driving the ecosystem response to nutrient injection. Nevertheless, observations show differential responses among a variety of plankton functional groups and size classes (see numerous references on the Georges Banks–Backus, 1987, Davis, 1984, 1987– and SOIREE experiment—Boyd and Law, 2001) that cannot be reproduced by such simple models. Indeed recent experimental and modeling studies in freshwater environment reveal that the overall ecosystem response to nutrient enrichment strongly depends on functional diversity (Hulot et al., 2000). Other studies based on observations and models show that the slope of the plankton size spectrum is very sensitive to vertical motion, biological parameterizations, and large-scale variability (Rodriguez et al., 2001; Martin and Srockoz, 2002). These results, in addition to the known importance of plankton size in controlling export production (e.g. large plankton cells are associated with strong export), motivate us to ask the following key question: Does the strong variability of the mesoscale and sub-mesoscale dynamics constrain the structure of plankton community and associated matter fluxes?

Two recent studies (Martin et al., 2001; Lima et al., 2002) addressed this question by incorporating two food web models, a single-species and a multi-species formulation, into a three-dimensional eddy-resolving model of an unstable frontal jet to investigate the effects of mesoscale instabilities on biological community structure in oligotrophic ocean environments. Different parameterizations of phytoplankton growth rates and phytoplankton loss terms lead to different conclusions. In their multi-species formulation, Martin et al. (2001) did not find significant differences in total plankton biomass and in the efficiency of nutrient utilisation compared to the single-species formulation. They observed a partition of biomass and fluxes between the two phytoplankton variables. On the contrary Lima et al. (2002) show that in the multi-species formulation nutrients are used more efficiently, resulting in higher total plankton biomass for the same amount of total nitrogen in the domain, notably outside the unstable front. As stressed by Lima et al. (2002), conclusions differ between these two studies mainly because of different formulations for phytoplankton growth rates and mortality rates.

In the present study we propose a new numerical process study in which our goal is not to address the comparison between single and multi-species models but to focus on the effects of sub-mesoscale dynamics on the phytoplankton competitions. For this purpose we have chosen one of the simplest model configurations permitting to address this question. This model includes two different phytoplankton groups in competition for one nutrient and controlled by one zooplankton, and one detritus compartment including remineralization and sedimentation. The configuration corresponds to an oligotrophic situation to focus on the combined effects of horizontal and vertical mechanisms on nutrient limitation, and we conduct coupled physical–biological simulations in a fully developed turbulent eddy field at statistical equilibrium. This is a noticeable difference from Martin et al. (2001) and Lima et al. (2002) who conducted short time coupled

simulations in which the results might depend on initial conditions. In our model the biological parameters which drive the phytoplankton competitions follow the work of Margalef (1979) on phytoplankton successions and are detailed in the next part. One question that has not been usually addressed in the literature concerns the effect of grazing pressure on the competition and coexistence of different phytoplankton groups (Franks, 2001). One aspect of the present study is to compare the effects of a realistic grazing pressure (what we call high grazing) with a low grazing pressure in the case of fine scale dynamical forcing. The low grazing pressure case is not a realistic case but gives insights on the phytoplankton competitions depending on the nutrients availability driven by the fine scale dynamics. It may be thought also as a way to isolate the effects of grazing by meso-zooplankton which is known to be weak, ignoring the grazing by micro-zooplankton.

The paper is organized as follows: the physical and biological models and parameter settings are presented in the following part. Then the effects of fine scale dynamics are described at the nonlinear statistical equilibrium with two different zooplankton parameter settings: a low grazing pressure and a high grazing pressure. In the next part we present a statistical analysis on the effects of fine scale dynamics and grazing on the ecosystem structure and functioning. The last part is the conclusion.

2. Model description

The Ocean circulation model used is the primitive equation (PE) model OPA (Madec et al., 1991, 1999; Foujols et al., 2000), in which a set of biological tracers has been embedded.

2.1. The dynamical model

The PE model is used in a configuration close to the one described in Rivière et al. (2004), except the resolution that is higher here. The effects of mesoscale and sub-mesoscale dynamics can be observed all over the oceans. Here, without loss of generality, we have chosen a configuration of our model that reproduces the dynamics of an eastern jet in the southern hemisphere during summertime. Most of the choices concerning the physical settings have been described and motivated in Rivière et al. (2004). So we refer the reader to this paper for more information and give here only the main features. The initial stratification that defines the initial baroclinically unstable current in thermal wind balance is indicated in Fig. 1. This stratification is associated with a mean deformation radius of 21 km. To initiate the instability, a small perturbation in wavenumbers 1–10 (relative to the channel length) is added to the temperature field. The nonlinear statistical equilibrium of an oceanic jet results from interactions between mesoscale eddies arising from baroclinic instability, large-scale meanders and the mean zonal flow (Karsten et al., 2002). A forcing mechanism is needed to achieve such an equilibrium. In the real ocean, wind forcing, differential heating and bottom topography play an important role. In order to isolate the effect of mesoscale and sub-mesoscale dynamics, we restrict ourselves to the flat-bottom case. In this context, the simplest forcing that allows the maintenance of a realistic baroclinic jet is relaxation to a mean density profile. We use such a relaxation towards initial temperature, with a relaxation time of 200 days. This time scale is large when compared with time scales associated with baroclinic instability as shown in Rivière et al. (2004). There is no net heat flux at the surface but we impose a solar

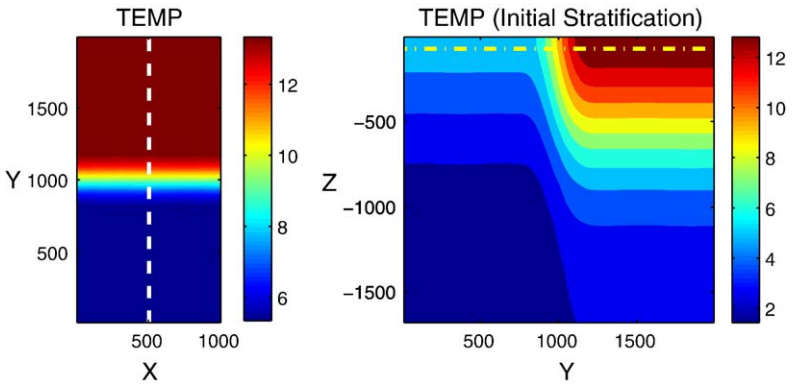

Fig. 1. Initial stratification of the primitive equation model. Left: sea surface temperature; right: vertical and meridional section of temperature (°C) along the dashed line indicated on the left panel. Initial mixed layer depth is also indicated. X and Y in km, Z in m.

penetration compensated by cooling at the surface so that a mixed layer depth of 50 m is maintained (Lévy et al., 2001). Salinity is held constant for simplicity, and a linear equation of state is used. Horizontal resolution is 6 km by 6 km, vertical resolution varies with depth: 36 levels spaced from 10 m in the first 200 m to 300 m at the bottom. Horizontal mixing of momentum and density is a classical biharmonic operator (with a coefficient equal to $5\cdot10^{10}\,m^4\,s^{-1}$) that is necessary for such a horizontal resolution to remove small-scale numerical noise induced by direct enstrophy cascade. For the vertical mixing, we use the classical second order closure of the model (Blanke and Delecluse, 1993). A vertical mixing background value is set to $10^{-5}\,m^2\,s^{-1}$. The geometry of the problem is a zonal channel, zonally periodic with walls at the north and south, on a β plane with $f_0=-10^{-4}\,s^{-1}$ and $\beta=1.6\cdot10^{-11}\,m^{-1}\,s^{-1}$. Zonal and meridional extensions are $L_X=1000$ km and $L_Y=2000$ km respectively. In particular the meridional extension is large enough compared with the initial width of the frontal region (300 km) and it has been checked that no effect of Northern or Southern boundary on the eddy dynamics is observed (Rivière et al., 2004). The depth is $H=4000$ m. Neither wind nor topography is introduced, which allows us to focus on the variability only induced by mesoscale and sub-mesoscale mechanisms. The physical model is integrated until a statistical equilibrium is reached (360 days) before activating the biological model.

We acknowledge here that previous studies dedicated to sub-mesoscale dynamics (Lévy et al., 2001 or Spall and Richards, 2000) have used a higher resolution than ours. The difference between these studies and the present study is that we are interested in statistically equilibrated systems that require long-term integration and a large domain. This is why we chose a lower resolution. With a deformation radius of 21 km that is eddies with diameters close to 70 km this resolution permits us to well resolve the mesoscale dynamics. The sub-mesoscale dynamics is characterized by structures 5 to 10 times smaller than mesoscale so the resolution does not fully resolves the filamentary dynamics but is able to capture its main characteristics. We emphasize that using a higher resolution should strengthen the differences revealed by our study between dynamics in mesoscale and filamentary regions.

2.2. The biological model

The biological model is adapted from the Nitrogen–Phytoplankton–Zooplankton–Detritus (NPZD) model used in Lévy et al. (2001). The modification consists of a differentiation of two prognostic variables for phytoplankton. Thus a total of five prognostic biological variables are considered: dissolved inorganic nitrogen (N), two phytoplankton classes (P_1 and P_2), one zooplankton (Z) and one detritus (D), all represented as equivalent scalar concentrations of Nitrogen (mmol m^{-3}). The structural relationships among the different biological variables are described by the model equations and coefficients values given in Tables 1 and 2 respectively. These biological variables are submitted to advection and vertical diffusion. The numerical advection scheme used for biological tracers (MUSCL) is different from the one used for temperature (see Lévy et al., 2001 for details). It is more diffusive and less dispersive than other classical schemes so that no horizontal diffusion is added on biological tracers (Lévy et al., 2001).

The potential limiting nutrient (N) is used by phytoplankton, and is regenerated either through remineralization of detritus or zooplankton excretion. Phytoplankton growth is a function of both light (I) and inorganic nutrient (N) availability. In the model, light

Table 1
Biological sources and sinks terms considered in the model

$$\mathring{N}=\tau D+\varepsilon Z-\mu_1\frac{N}{K_{N1}+N}\left(1-e^{-I/K_{I1}}\right)P_1-\mu_2\frac{N}{K_{N2}+N}\left(1-e^{-I/K_{I2}}\right)P_2$$

$$\mathring{P}_1=\left[\mu_1\frac{N}{K_{N1}+N}\left(1-e^{-I/K_{I1}}\right)-m_P\right]P_1-g_1\frac{p'_1P_1}{K_{Z1}+F}Z$$

$$\mathring{P}_2=\left[\mu_2\frac{N}{K_{N2}+N}\left(1-e^{-I/K_{I2}}\right)-m_P\right]P_2-g_1\frac{p'_2P_2}{K_Z+F}Z$$

$$\mathring{Z}=\left[g_1\left(\beta_1\frac{p'_1P_1+p'_2P_2}{K_Z+F}+\beta_2\frac{p'_3D_1}{K_ZF}\right)-\varepsilon-m_ZZ\right]Z$$

$$\mathring{D}=\left[g_1\left((1-\beta_1)\frac{p'_1P_1+p'_2P_2}{K_Z+F}+(1-\beta_2)\frac{p'_3D}{K_ZF}\right)+m_ZZ\right]Z+m_P(P_1+P_2)-\tau D-g_1\frac{p'_3D}{K_Z+F}Z$$

with

$$p'_1=\frac{p_1P_1}{p_1P_1+p_2P_2+p_3D},\ p'_2=\frac{p_2P_2}{p_1P_1+p_2P_2+p_3D},\ p'_3=\frac{p_3D}{p_1P_1+p_2P_2+p_3D}$$

and

$$F=p'_1P_1+p'_2P_2+p'_3D$$

The dot represents the time derivative. Parameter significations and values are given in Table 2.

Table 2
Values of the model coefficients corresponding to equations detailed in Table 1

Symbol	Values	Unit	
Phytoplankton			
μ_1, μ_2	1.33, 2.00	day^{-1}	Maximal phytoplankton growth rate
K_{N1}, K_{N2}	0.15, 0.60	mmol N m^{-3}	Half saturation constant for nutrient uptake
K_{I1}, K_{I2}	37.50, 25.77	µEinst m^{-2} s^{-1}	Affinity for light
m_P	0.035	day^{-1}	Mortality rate
Zooplankton			
g_1	1.00	day^{-1}	Maximal ingestion rate
K_Z	0.90	mmol N m^{-3}	Half saturation constant for ingestion
p_1, p_2, p_3	0.3333		Preference for P_1, P_2 and D
β_1, β_2			Assimilation efficiency for P_i and D
	0.2, 0.3		For Low Grazing model
	0.8, 0.7		For High Grazing model
m_Z	0.01	day^{-1} mmol N^{-1}	Shape of the mortality curve
ε	0.07	day^{-1}	Excretion rate
Detritus			
τ	0.10	day^{-1}	Specific remineralization rate
V	5 m	day^{-1}	Detritus sinking rate

intensity at the sea surface, represented by Photosynthetic Available Radiation (PAR), is assumed to be a constant (150 W m^{-2}). Its penetration into the ocean is governed by a simplified version of Morel's (1991) algorithm, in which two wavelengths (red and blue) are considered. In the simulations performed in this study the initial euphotic depth is close to 150 m (defined as the 1% light level). This depth of 150 m may be thought as the potentially highlighted layer during the simulations, and it has been chosen to calculate the vertical average of all the biological fields at the equilibrium.

For studying competitions between P_1 and P_2, one of the most important points is how they are differentiated. Margalef shows that phytoplankton seasonal successions are often characterized by a shift from cells adapted to low-light and high-nutrients conditions to cells adapted to high-light and low-nutrients conditions. In addition, it is often observed that cells actively growing in conditions of high nutrient concentration and weaker stability of the water column, such as diatoms, have higher maximal growth rates than cells growing in conditions of low nutrient and strong stability of the water column such as dinoflagellates (see for example Banse, 1992). In our model the coefficients which drive phytoplankton growth rates are simply parameterized using traditional Michaelis-Menten formulation for phytoplankton growth. Here P_1 and P_2 differ by their maximal growth rate (μ_{Pi}) and their relative affinity for light (K_{Ii}) and nutrients (K_{Ni}). The realized specific growth rate is thus written:

$$\mu_i = \mu_{Pi} \times \frac{N}{K_{Ni} + N} \times \left(1 - \exp^{\left(-\frac{I}{K_{Ii}}\right)}\right)$$

In our study, phytoplankton coefficients were chosen so that P_1 and P_2 represent two types of phytoplankton, adapted either to low-nutrient and high-light conditions such as dinoflagellates (P_1), or to high-nutrients and low-light conditions as diatoms (P_2). More precisely P_2 has a maximum growth rate of 2 day^{-1} characteristic of diatoms (Blasco et al., 1982) whereas the maximum growth rate of P_1 in our study is slightly lower (1.33 day^{-1}) as usually observed for nano- and pico-phytoplankton (Kana and Glibert, 1987). So, in the model, the phytoplankton variable with the highest affinity for nutrients and the lowest affinity for light has also the lowest maximal growth rate. The ratio μ_2/μ_1 is represented in Fig. 2 as a function of N and I: in our simulations P_1 will be competitive only in oligotrophic conditions (N<0.5 mmol m^{-3}).

Phytoplankton loss terms are represented by natural mortality and grazing. In the grazing functional response, the preference for food sources changes as a function of the relative proportion of each resource (Fasham et al., 1990). Zooplankton grazes on both phytoplankton and detritus, with an equal coefficient of preference for each resource P_i (Table 2). Zooplankton loss terms are due to production of faecal pellets, excretion and mortality. Detritus are produced by

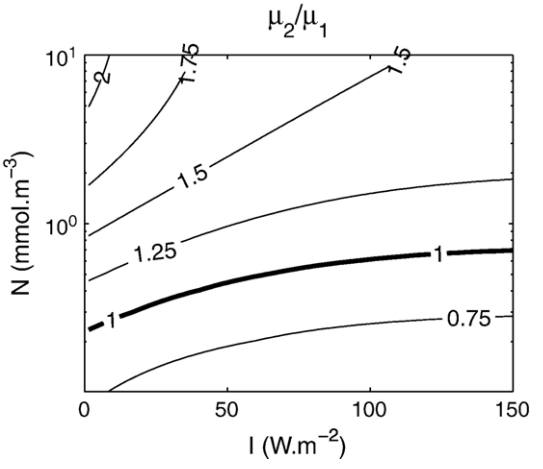

Fig. 2. Ratio between realized growth rates of P_1 and P_2 as a function of light intensity (I) and nitrogen concentration in nutrients (N).

mortality of phytoplankton and zooplankton or by egestion. The detritus loss terms are represented by grazing, remineralization and sinking. It is important to notice here that the only variable that sinks in the model is detritus.

One important aspect of the modeling approach developed here concerns the comparison between two grazing scenarios. This comparison is motivated by our aim to better understand the respective impact of food-web structure and fine scales dynamics on the ecosystem response to nutrient injection. To date, most of the coupled physical–biological model consider zooplankton as a prognostic state variable because "it has to be there", which is of course true. Here we also consider zooplankton, but we compare a simulation in which it is prevented from developing by assuming a very low assimilation efficiency, subsequently referenced to as Low grazing model, to a simulation in which we let zooplankton to develop, referenced to as High Grazing model (see Table 2). The underlying idea is to have a first order idea of how the ecosystem responds to nutrient injection when dominant grazers are not able to prevent phytoplankton from blooming. This might occur, for example, in situations where large diatom blooms are weakly controlled by either micro-zooplankton or mesozooplankton grazing pressure. Both the low grazing model and the high grazing model are coupled to the physical model OPA by advection and diffusion, using either a high horizontal resolution (HR-simulation) of 6 km, or a low horizontal resolution (LR-simulation), which prevents the development of mesoscale dynamics (a horizontal resolution of 50 km and a high harmonic viscosity). This latter can be thought as the unperturbed case by which we can gauge the impact of mesoscale turbulence. The comparison between the four different models (Low Grazing–Low Resolution, Low Grazing–High Resolution, High Grazing–Low Resolution, and High Grazing–High Resolution) gives some first-order ideas on the respective roles of food-web structure and fine scale dynamics on the ecosystem response to nutrient injections. Initial conditions for the low resolution model are performed with an analytical exponential vertical profile of nutrients characteristic of oligotrophic regions (from 0.1 at the surface to 30 mmol N m^{-3} at the bottom with a nutricline close to 100 m), the other biological variables being initialized to a constant equal to 0.1 mmol N m^{-3}. Initial conditions for the high resolution model are performed for the nutrient from the field predicted by the low resolution simulation, the other biological variables being initialized to a constant equal to 0.1 mmol N m^{-3}.

3. Ecosystem responses to fine scale dynamics at the statistical equilibrium

3.1. Dynamical fields

The surface temperature at the nonlinear statistical equilibrium is presented in Fig. 3a (at day 815 of the nonlinear simulation with the high resolution model). This temperature distribution is characteristic of geostrophic turbulence associated with unstable large-scale oceanic fronts. A fully developed mesoscale eddy field is observed at north and south of the zonal mean circulation. This dynamics is mainly induced by the baroclinic instability of the mean circulation (see Rivière et al., 2004 for details) and is characterized by large-scale meanders in the main current (wavelength from 200 to 500 km) and mesoscale eddies detaching from this circulation at north and south with horizontal radii around 100 km. Around these eddies small-scale structures are also observed in the temperature field resulting from the classical inverse cascade towards small scales driven by the eddy deformation field. This fine scale dynamics is clearly revealed by the surface vorticity field in Fig. 3b. Indeed the variability of the vorticity is not only characterized by mesoscale structures (cyclones and anticyclones) but also by filamentary structures, at sub-mesoscale, whose width is from 30 to 60 km. This dynamics appears to be preponderant at south of the jet compared with north where eddies are larger and less numerous. A 2D spectral analysis (not shown) reveals a spectra slope close to K^{-1} for the surface vorticity (where $K=(k^2+l^2)^{1/2}$ is the total wavenumber) and K^{-2} for the surface temperature according to previous studies (Klein et al., 1998). In the next parts we will refer to "mesoscale region" the region situated close to the central frontal region (dominated by mesoscale dynamics characterized by structures of the order of 70 km and more) and to "filamentary region" the adjacent region situated south (dominated by sub-mesoscale dynamics characterized generally by structures 5 to 10 times smaller than mesoscale structures).

The vertical velocity distribution at 150 m (Fig. 3c) reveals alternatively large up- and downwellings associated with meanders in the front (up to ±30 m per day). Out of the front the vertical velocities are weaker (several meters per day) but are situated into the vorticity filaments (upwellings mainly into positive vorticity regions and downwellings into negative vorticity regions). The magnitude of the vertical motion is small compared with observations mainly into filaments, but this is a trait of most models except models with very high resolution (Lévy et al., 2001). We thus would like to

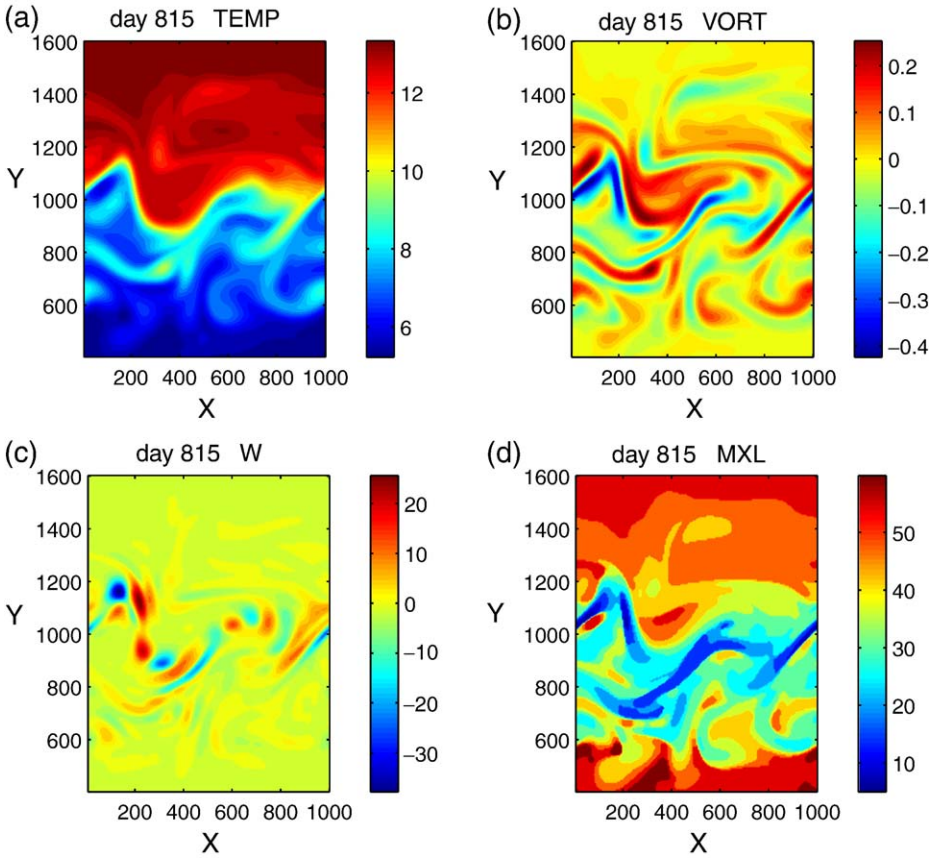

Fig. 3. Instantaneous snapshots of dynamical fields at day 815 in the High Resolution–Low Grazing simulation: (a) surface temperature (°C), (b) surface relative vorticity (10^{-4} s^{-1}), (c) vertical velocity (m day^{-1}) at 150 m, and (d) mixed layer depth (m). These figures (as all the figures hereafter) show a zoom on the turbulent region from 400 km to 1600 km in the meridional direction. The regions at north and south of the domain close to the frontiers are not shown for convenience of the reader, but we have checked that they are unaffected by mesoscale dynamics.

emphasize here that the results of the present study would be more marked in the reality as a consequence of stronger vertical transport. All this variability affects the mixed layer depth that is submitted to advection. Mixed layer depth distribution reveals filamentary structures associated with strong horizontal gradients (several tens of meters over a few tens of kilometers).

Let us consider now how does this fine scale dynamics impacts the ecosystem structure at the nonlinear statistical equilibrium.

3.2. Low grazing simulation

3.2.1. Horizontal and vertical distribution of chemical and biological variables

Fig. 4 shows the ecosystem structure at the statistical equilibrium when the grazing pressure is low. The day chosen in this figure is representative of the features observed during the simulation at the equilibrium. We observe first a filamentary biomass and nutrients distribution. A maximum of biomass variability is observed in the filamentary region (between 450 km and 900 km in the meridional direction) with small-scale signature. Into the mesoscale region, close to 1000 km, the biomass distribution is also filamentary with high maxima but organized along the meanders.

The relative measure of the phytoplankton dominance $\alpha=(P_2-P_1)/(P_2+P_1)$, where P_2 and P_1 are the nitrogen concentrations averaged over the initial euphotic depth, is shown in Fig. 4e. In this simulation P_2 dominates everywhere but the spatial distribution of α reveals a strong variability. In particular, in the filamentary region, the largest α values close to 0.9 are mostly located into nutrient rich filaments, whereas the lowest α values close to 0.7 are situated in low nutrient regions between filaments. Within the mesoscale region, in the central frontal region, the values of α vary less, with values close to 0.9, denoting a large dominance of P_2.

In the filamentary region the response of the ecosystem is depicted in Fig. 5 which shows a zoom of P_1, P_2 and N on a small area in this region around a cyclonic eddy and associated filaments. It reveals that the

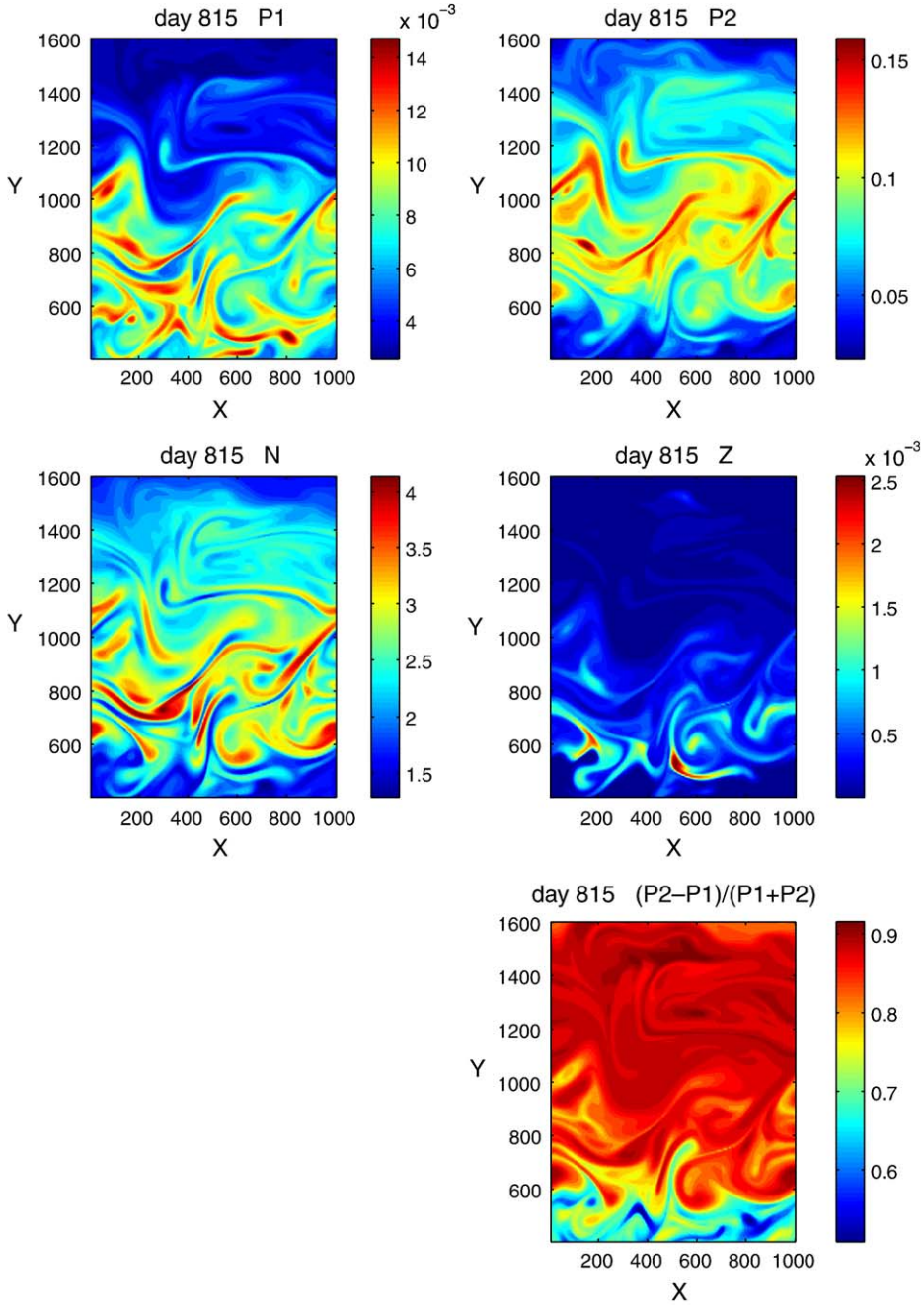

Fig. 4. Instantaneous snapshots of biological fields at day 815 in the Low Grazing simulation: P_1, P_2 N and Z (mmol N m^{-3}) averaged over the initial constant euphotic depth (150 m) and relative dominance of phytoplankton $\alpha=(P_2-P_1)/(P_2+P_1)$. The zooplankton is indicated for information: it does not emerge significantly in this simulation. Be aware of the difference of scales in color bars between P_1 and P_2: the ratio between P_1 and P_2 is of the order of 10.

sub-mesoscale dynamics in this region induces a spatial segregation of the two phytoplankton classes: P_2 maxima are observed in high nutrients structures and minima in other places, whereas P_1 is inversely distributed. This is coherent with the spatial distribution of the relative dominance α (Fig. 4e). This spatial segregation is not observed in the mesoscale region, and we emphasize here that the difference in the ecosystem response between mesoscale and filamentary regions is not due to solar radiation, nutricline depth or mixed layer depth because all these quantities are initially invariant from north to south. It is only due to the sub-mesoscale

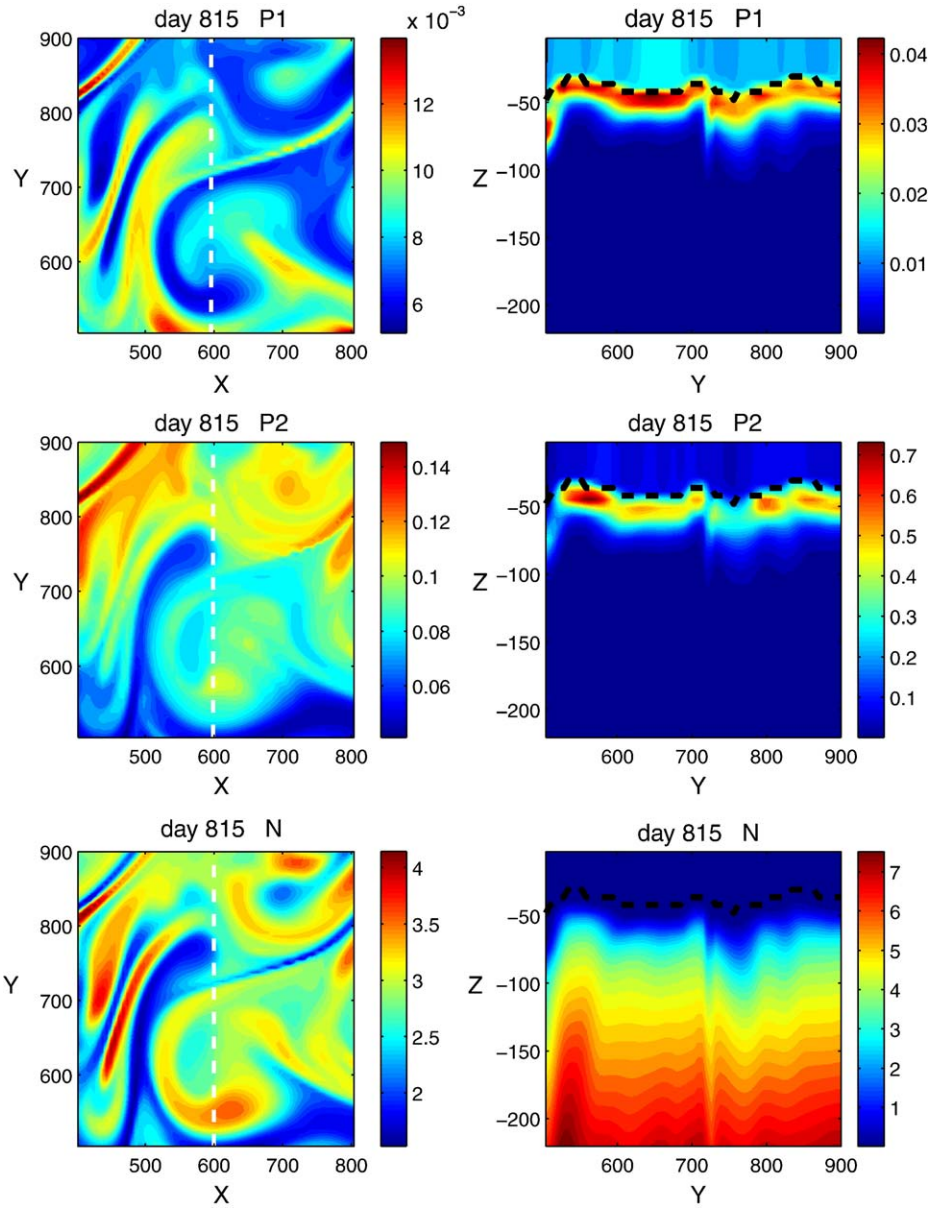

Fig. 5. On the left panels: horizontal distribution of P_1, P_2, and N averaged over 150 m (mmol N m^{-3}) into filamentary region in the southern part of the domain in the Low Grazing pressure simulation. On the right panels, vertical distribution of P_1, P_2, and N along the radial indicated on the left panels. Dashed line indicates mixed layer depth.

dynamics that dominate south of the central frontal region. Fig. 5 also presents the vertical section of phytoplankton and nutrients. We see that the model reproduces a thin subsurface biomass maximum (DCM) located under the base of the mixed layer. This DCM appears to be very patchy with strong signature of filamentary structure of the biomass. We observe also that these maxima of biomass are strongly related with vertical inputs of nutrients. Maxima of biomass, located for P_2 into filaments, are observed at the base of the nutricline that is pushed upward, very close to mixed layer base in these regions.

3.2.2. Scatter plots of biological and physical fields

Fig. 6a shows the scatter plots of P_1 versus P_2 in the filamentary and mesoscale regions. It confirms the difference in the spatial distribution of the phytoplankton between these two regions. In the filamentary region the slope of the scatter plot indicates clearly that maxima of P_2 are related to minima of P_1 and inversely, whereas in

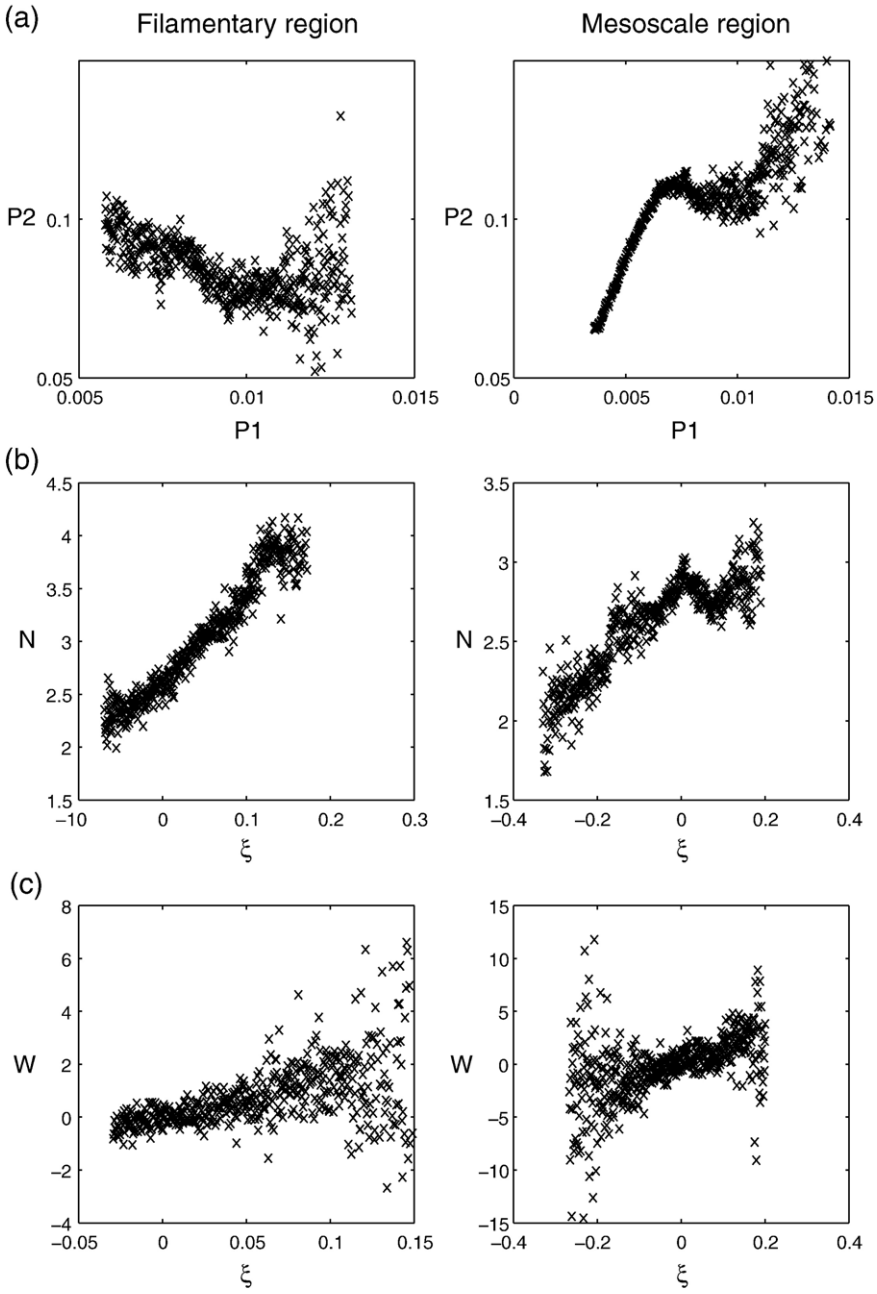

Fig. 6. Scatter plots of (a) P_2 and P_1 (averaged over 150 m), (b) N and ξ (where ξ is the surface relative vorticity, and N is averaged over 150 m), (c) W and ξ (where W is the vertical velocity at 150 m) over two different regions at day 815 in Low Grazing simulation. Left: over the filamentary region (from 500 km to 800 km in the meridional direction), right: over the mesoscale region (from 800 km to 1200 km in the meridional direction). Units: mmol N m^{-3} for N, P_1 and P_2, m day^{-1} for W and 10^{-4} s^{-1} for ξ.

the mesoscale region the slope is reversed showing a strong relation between the two phytoplankton class distributions.

Fig. 6b–c shows the relation between nutrient concentration, vorticity and vertical velocity. In the two regions under focus, these relations are very similar and reveal strong correlations between these different quantities. More precisely high nutrient regions are located in positive vorticity structures whereas low nutrient regions are located in negative vorticity regions, and extrema of vorticity are associated with extrema of vertical velocities. These results are in agreement with

the statistics calculated in Lévy and Klein (2004) in a northern hemisphere configuration. Now, although the correlation between nutrients and dynamics are similar in both regions (Fig. 6bc), the biological response differs from one region to the other (Fig. 6a).

Let us consider first the filamentary region. The relation between vorticity and vertical motion in this region (Fig. 6b) is in accordance with Hakim et al. (2002) who shows that the mechanisms involved during the emergence of filamentary structures are associated with local vertical motions due to frontogenesis mechanisms (see their Fig. 11). These vertical motions are related to convergence or divergence depending on the vorticity and temperature. Our results reveal that this mechanism may explain high nutrient concentrations observed into positive vorticity filaments (Fig. 6c) through vertical injections into filaments submitted to stirring mechanism. Our interpretation of the spatial segregation of phytoplankton observed in Fig. 6a is as follows: because of the parameter choices for P_1 and P_2 (see Fig. 2), into the nutrient-rich filaments, P_1 is competitively excluded. Outside these structures, where nutrients are less abundant, the competition is weaker and P_1 is able to develop. We have checked (figure not shown) that on these scatter plots the maximum values of P_2 (and minimum values of P_1) are associated with maximum of nutrients integrated over the euphotic layer, upward vertical nutrient fluxes and also positive vorticity, whereas minimum values of P_2 (and maximum values of P_1) are associated with minimum of nutrients, mostly downward vertical nutrient fluxes and also with negative vorticity.

In the mesoscale region the phase relationship between vertical and horizontal motions is different. Indeed these quantities are mainly related to mesoscale dynamics involving wave mean flow interactions and baroclinic instability and characterized by strong convergent and divergent motions. We suspect that the higher vertical fluxes in this region and also the larger scales involved make the competition between P_1 and P_2 less unfavourable to P_1. In particular we have verified that the most linear part of the scatter plot in Fig. 6a, corresponding to low P_1 and P_2 values, correspond to high upward nutrient fluxes, whereas the other part corresponding to high P_1 and P_2 values is associated with mostly high downward nutrient fluxes (figure not shown). We have subsequently calculated that, in this mesoscale region, the time scale related to horizontal convergences (calculated simply as the inverse of the divergence of the horizontal velocity) is around 1–2 days that is of the same order as the mean realized growth rate over the surface layers. This may explain why the maximum of biomass is observed in low nutrient zones associated with convergent motions contrarily with the filamentary region. This effect of convergence into a frontal region which constrains the biomass distribution has been already observed in the Antarctic Polar Front by Strass et al. (2002), and also reported in a preceding numerical study in the ACC (Hense et al., 2003). The main mechanism argued by these authors was that the newly upwelled water, rich in nutrients but poor in phytoplankton, is advected horizontally near the surface and phytoplankton grows until water is downwelled.

3.3. High grazing simulation

3.3.1. Horizontal and vertical distribution of chemical and biological variables

Fig. 7 shows the same fields as in Fig. 4 but for the high grazing simulation. The same filamentary characteristics are observed in the biomass as in the low grazing simulation but now the zooplankton emerges significantly and controls the phytoplankton community structure. In particular the vertical mean concentration for P_2 is strongly decreased compared with low grazing case, and P_1 increases in such a manner that P_2 is now of the same order of magnitude as P_1. The relative dominance α is significantly modified by the grazing pressure: its values are globally decreased and are now negative in some regions indicating a dominance of P_1. In the whole turbulent region (between 500 km and 1400 km in the meridional direction) the competition between the two phytoplankton classes is more active and a co-dominance is observed in many places. However P_2 always dominates in high nutrient filamentary structures as in the low grazing simulation. The zooplankton emerges into filamentary structures also, and specifically into regions where P_2 was largely dominant in the low grazing simulation. In contrast to the strong effect of grazing of phytoplankton, we notice that the nutrient field is quasi unaffected by the grazing.

A zoom on filaments in the southern region (Fig. 8) reveals that the emergence of P_1 inside the high nutrient filaments has been increased compared with the low grazing case. This is particularly observed on the vertical cross section. Now P_2 and P_1 have much closer spatial distribution with a significant increase of biomass into filaments. But P_1 is always competitive into low nutrients structures as in the low grazing case. The vertical sections reveal also that the grazing reduces the vertical extension of the subsurface chlorophyll maximum that is now closer to the mixed layer base.

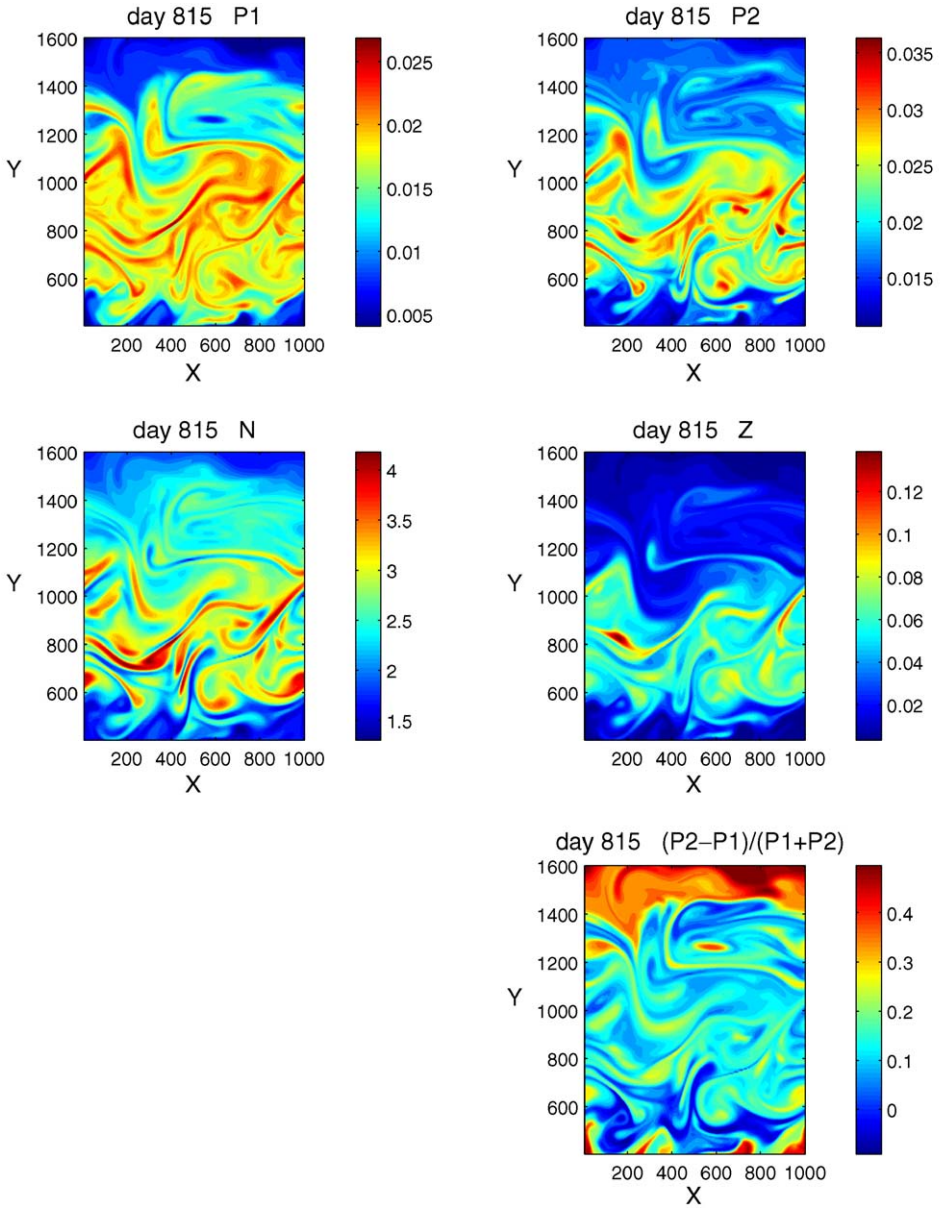

Fig. 7. Biological fields (P_1, P_2, N and Z) and phytoplankton relative dominance $\alpha=(P_2-P_1)/(P_2+P_1)$ in the High Grazing simulation at the same day as in Fig. 4. Units: mmol N m^{-3}.

3.3.2. Scatter plots of biological and physical fields

Scatter plots of P_1 versus P_2 in Fig. 9 indicate also a strong modification of the relation between the two phytoplankton spatial distributions compared with low grazing simulation: in the filamentary region the slope is now positive indicating that grazing tends to inhibit the spatial segregation between phytoplankton classes. More precisely high grazing pressure prevents each phytoplankton group from being largely dominant. Indeed, in the mesoscale region the slope of the scatter plot is now closer to 1, which reveals co-dominance between P_1 and P_2. A similar slope is observed in the filamentary region, where the competitiveness of P_2 is now limited by the grazing pressure despite nutrient injections into filaments.

3.4. Spatial correlations

In the preceding paragraphs the relations between phytoplankton in different regions with low and high grazing have been depicted with the mean of scatter plots. In particular a spatial segregation has been depicted in the

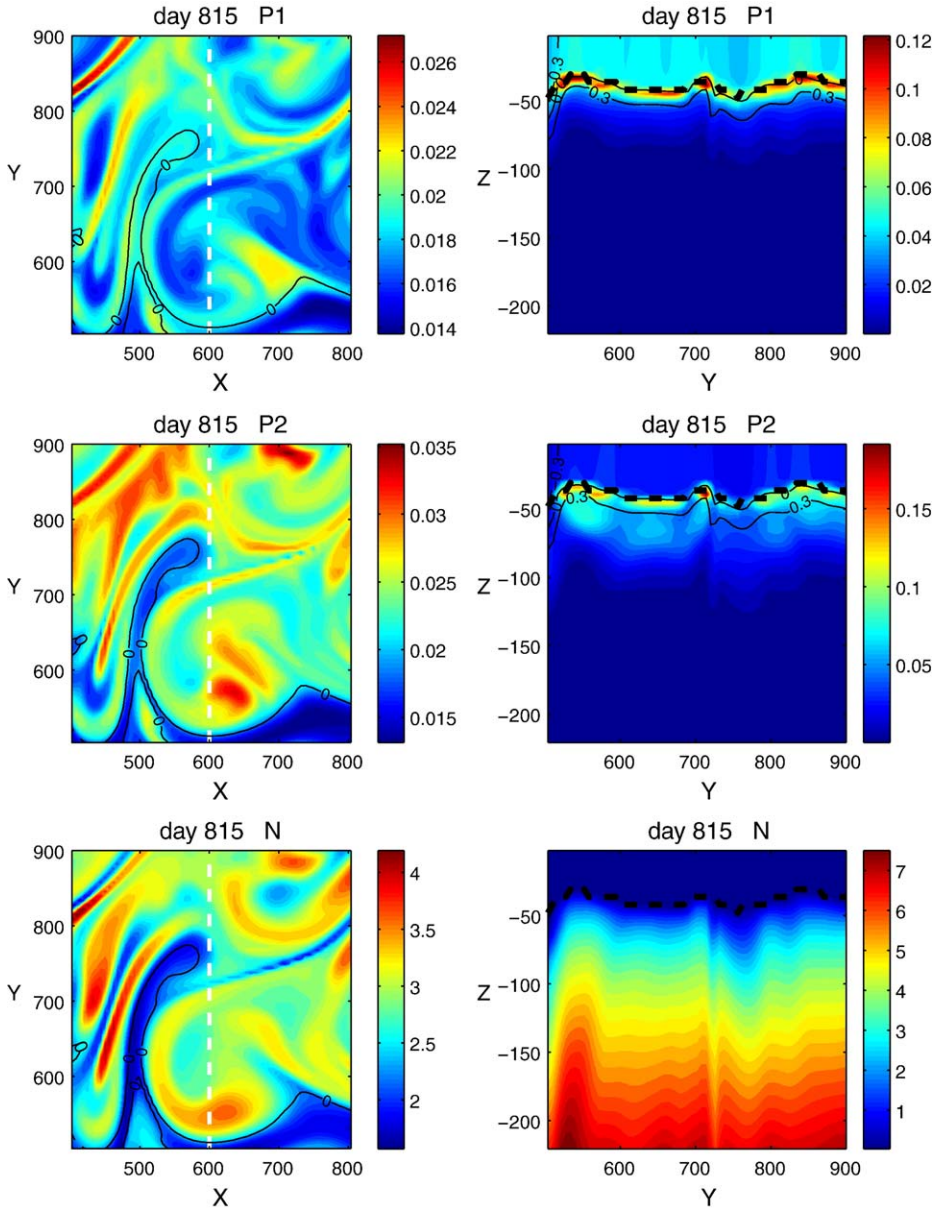

Fig. 8. Same as Fig. 5 but for High Grazing simulation. Lines indicate the values of the relative dominance α.

filamentary region. To comfort these results we have calculated in Table 3 some spatial correlations in the two different regions (the filamentary region between 500 km and 800 km, and the mesoscale region between 800 km and 1200 km) for the low and high grazing models at the statistical equilibrium. Let us consider first the correlations involving phytoplankton and nutrients. A low grazing pressure induces an anti-correlation of −0.3 between the two phytoplankton classes in the southern area. In this case P_2 is strongly correlated with nutrients (0.8) whereas an anti-correlation is observed for P_1 (−0.4). With high grazing the correlation between P_2 and P_1 switches to a significant positive value (0.7) in this area, associated with a positive correlation of P_1 with N. The correlation between P_2 and N is not affected by grazing. The different correlations are less sensitive to grazing in the mesoscale region: we observe a significant correlation between P_1 and P_2 and a low correlation between phytoplankton and nutrients.

Some mean correlations between phytoplankton and physical fields are also presented in Table 3, calculated

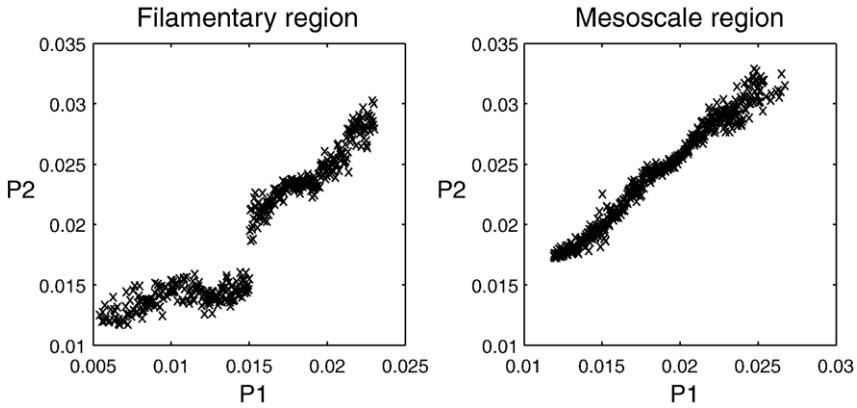

Fig. 9. Scatter plots of P_2 and P_1 (mmol N m^{-3}) over two different regions at day 815 in the High Grazing simulation. Left: filamentary region (from 500 km to 800 km in the meridional direction), right: mesoscale region (from 800 km to 1200 km in the meridional direction).

over the simulation at the statistical equilibrium. These statistics comfort our attempt of explanation of the spatial segregation of phytoplankton in the low grazing simulation: in the filamentary region a negative correlation is observed between P_1 and P_2. P_2 is positively correlated with relative vorticity (+0.3) and temperature (+0.8), whereas negative correlations are obtained with P_1 (−0.5). Nutrients are significantly correlated with P_2 (+0.8) and negatively correlated with P_1 (−0.4).

In the mesoscale region, the correlation between phytoplankton and temperature or vorticity is always significant and negative. In this region the correlation between phytoplankton and vertical velocity (not shown) is weak but slightly negative (close to −0.2). These results emphasize the role of the horizontal advection in the distribution of the biomass: maximum of biomass is generally not observed in the upwelling regions.

4. Some statistics on the effects of frontal dynamics and grazing

In this part we discuss the effects of frontal fine scale dynamics comparing the preceding high resolution simulations with low resolution simulations. The low resolution model, in which baroclinic instability is prevented to develop, can be thought as a perfect gauge by which the effects of mesoscale can be highlighted: only vertical diffusion and large-scale dynamics are able to drive significantly the biological tracers. For each resolution we compare the effects of low and high grazing pressures.

Table 3
Spatial correlations calculated over two areas: the filamentary region between 500 km and 800 km, and the mesoscale region between 800 km and 1200 km

Correlations between	Filamentary region		Mesoscale region	
	Low Grazing	High Grazing	Low Grazing	High Grazing
P_1 and P_2	−0.3 (σ=0.07)	0.7 (σ=0.07)	0.7 (σ=0.05)	0.8 (σ=0.04)
P_1 and N	−0.4 (σ=0.1)	0.3 (σ=0.09)	−0.2 (σ=0.1)	−0.1 (σ=0.08)
P_2 and N	0.8 (σ=0.04)	0.8 (σ=0.1)	0.1 (σ=0.05)	0.2 (σ=0.07)
P_1 and T	−0.5 (σ=0.05)	0.2 (σ=0.01)	−0.9 (σ=0.1)	−0.5 (σ=0.1)
P_2 and T	0.8 (σ=0.04)	0.6 (σ=0.1)	−0.5 (σ=0.07)	−0.5 (σ=0.1)
P_1 and ζ	−0.5 (σ=0.1)	−0.1(σ=0.02)	−0.8 (σ=0.1)	−0.6 (σ=0.1)
P_2 and ζ	0.3 (σ=0.08)	0.2 (σ=0.1)	−0.6 (σ=0.06)	−0.5 (σ=0.1)
N and ζ	0.6 (σ=0.09)	0.6 (σ=0.09)	0.4 (σ=0.08)	0.4 (σ=0.09)
W and ζ	0.5 (σ=0.08)	0.5 (σ=0.08)	0.3 (σ=0.05)	0.3 (σ=0.05)
T and ζ	0.5 (σ=0.1)	0.5 (σ=0.1)	0.7 (σ=0.02)	0.7 (σ=0.02)

The values indicated in this table have been averaged over 100 days at the statistical equilibrium. The values of the standard deviation σ are indicated in the table and never exceed 0.1. The significance of these spatial correlation coefficient has been checked. The fields P_1, P_2 and N are averaged over 150 m, the temperature T and vorticity ζ are taken at the surface, and the vertical velocity W is taken at the base of the initial euphotic layer (150 m).

4.1. Mean vertical profiles of dominance in low resolution (LR) versus high resolution (HR) simulations

Fig. 10 presents the vertical profile of the relative dominance α averaged in time at the statistical equilibrium. We observe that mesoscale dynamics produced by high resolution model globally increases the large phytoplankton competitiveness in surface layers but decreases it in subsurface in the two grazing cases. But one striking result is that the effect of grazing pressure is considerably increased by the mesoscale and sub-mesoscale dynamics. At low resolution the effect of grazing is weak and tends to recall the ecosystem towards an equal partition between the two phytoplankton classes: it reduces the dominance of P_1 in surface layer and inversely reduces the dominance of P_2 in subsurface. This can be explained by the parameterization of the zooplankton relative preferences which induces a shift from one resource to the other depending on their relative abundance. This parameterization keeps both phytoplanktons from dominating the community in the absence of advection. At high resolution, the effect of increasing grazing pressure is much more significant. In the surface layer (down to 40 m) it induces a shift in phytoplankton community from P_2 to P_1. Below the mixed layer the grazing pressure decreases the dominance of P_2 but keeps it dominant. This effect decreases with depth with no quasi effect at the base of the euphotic zone. The mean value of the dominance over each region is similar to Fig. 10 and is not shown, but the variance of this parameter is different with higher values in the filamentary region than in the mesoscale region, especially when grazing is low (not shown). This emphasizes the effect of filamentary dynamics on the ecosystem structure variability.

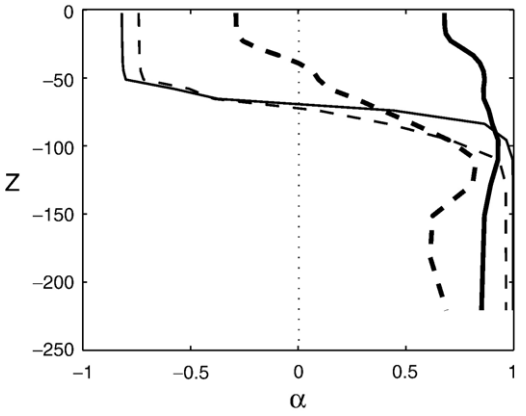

Fig. 10. Effects of small scales on the vertical structure of the ecosystem: vertical profile of the relative dominance $\alpha=(P_2-P_1)/(P_2+P_1)$. α is calculated at each depth with the horizontal mean of P_1 and P_2 concentrations. Thin line: low resolution; heavy line: high resolution; continuous line: low grazing pressure, dashed line for high grazing pressure.

Table 4
Mean values of nitrogen concentration in the biological model (mmol N m^{-3}), and of primary production (PP) and export (EXP) in mmol N day^{-1} with different horizontal resolutions and grazing pressures (average over the domain and the initial euphotic layer (150 m))

	LR–LG	LR–HG	HR–LG	HR–HG
P_1	0.001	0.010	0.005	0.011
P_2	0.029	0.015	0.059	0.018
P_1+P_2	0.030	0.025	0.064	0.029
Z	3.10^{-4}	0.013	2.10^{-4}	0.025
D	0.01	0.010	0.024	0.013
N	1.48	2.14	2.16	2.22
PP_1	$4.8\cdot10^{-5}$	$8.4\cdot10^{-4}$	0.0002	0.0014
PP_2	0.00144	0.00135	0.0029	0.0020
PP_1+PP_2	0.0015	0.0022	0.0031	0.0034
EXP	0.043	0.053	0.12	0.069

4.2. Some statistics comparing LR and HR simulations

Table 4 details the respective effects of horizontal resolution and grazing variations. Taking into account meso- and sub-mesoscale physics leads to a general increase of both stocks and fluxes. In the low grazing model the phytoplankton biomass (P_1+P_2) increases by 94%, the primary production increases by 118% and the export of detritus increases by 200%. Note that this increase mainly benefits to P_1 (+900%) rather than to P_2 (+110%). Using the high grazing model the trend is similar, although the increase is much weaker for biomass and export (+16% for biomass, +112% for primary production and +38% for export). Moreover, in this case, the increase is similar for P_1 and P_2 (+22% and +12%, respectively).

Looking more closely at the effects of grazing (the resolution being kept constant) gives us more information on the impact of zooplankton on ecosystem functioning. In the low resolution simulation, using the high grazing model rather than the low grazing model leads to a decrease of biomass (−24%), an increase of primary production (+13%) and an increase of export (+25%). In the high resolution simulation, biomass strongly decreases (−55%), primary production still slightly increases (+10%) but, contrary to the low resolution, export significantly decreases (−42%). Here, we interpret these contrasting effects of grazing depending on resolution as a result of the increasing residence time of detritus within the euphotic zone, through grazing of detritus by zooplankton. This higher

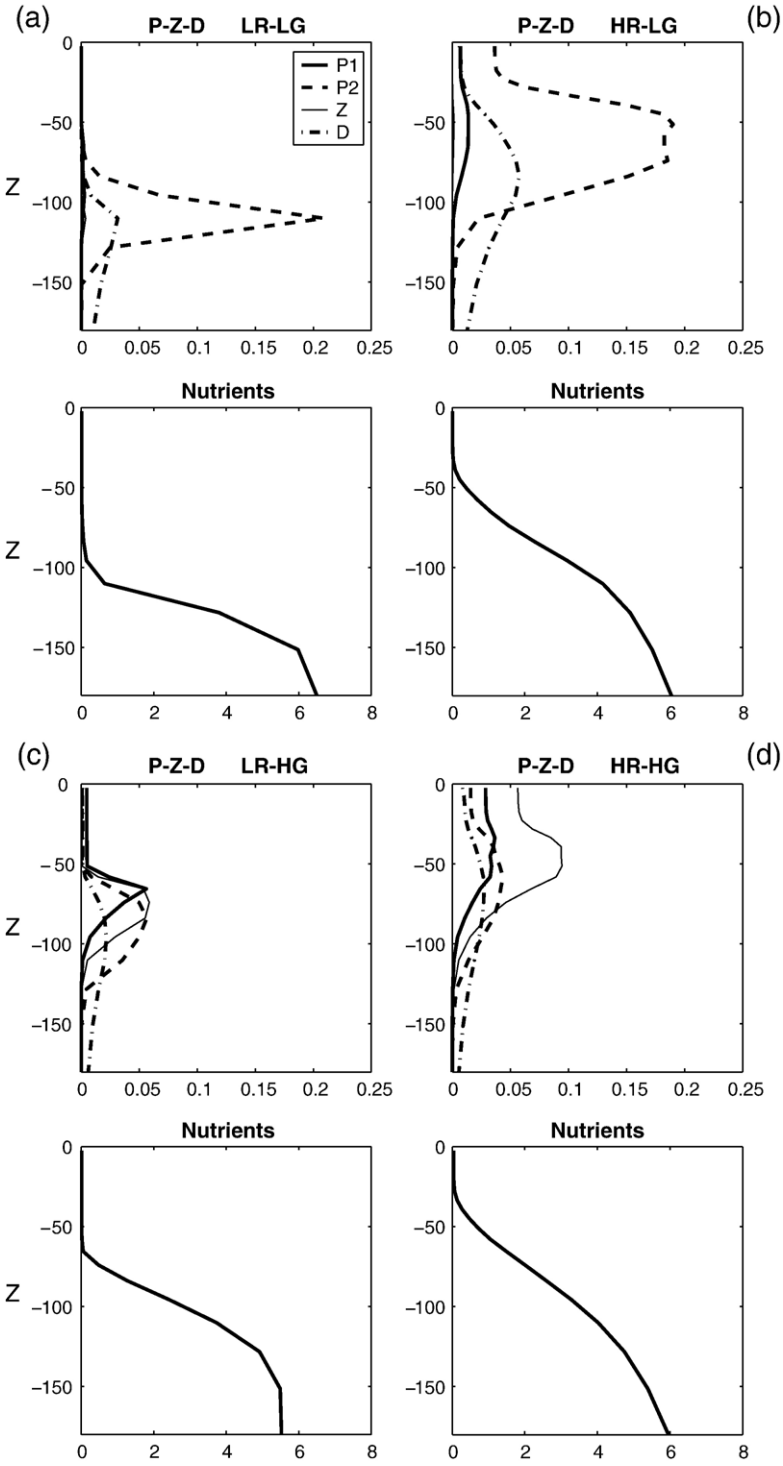

Fig. 11. Mean vertical profiles of P_1, P_2, Z, D and N (mmol N m^{-3}) at the statistical equilibrium in the four simulations: (a) Low Resolution–Low Grazing pressure, (b) High Resolution–Low Grazing pressure, (c) Low Resolution–High Grazing pressure, (d) High Resolution–High Grazing pressure.

residence time of detritus leads to higher regenerated production (through remineralization and zooplankton excretion), and lower export. In the high resolution simulation, the residence time of detritus is even higher within the mesoscale region, because of the upward vertical motion (around 10 m day^{-1}) which may

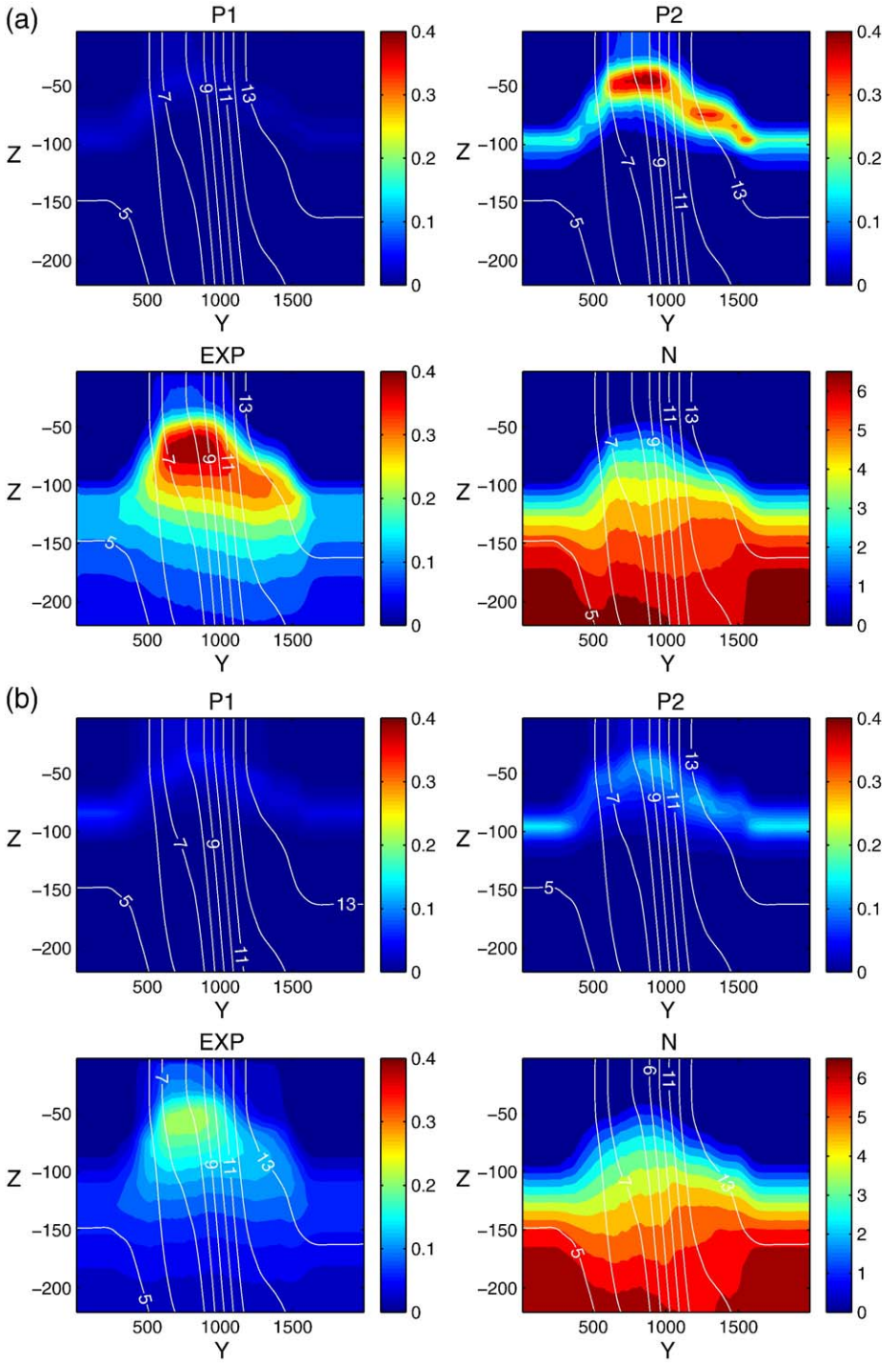

Fig. 12. Zonal mean cross sections of P_1, P_2, N (mmol N m^{-3}) and export (mmol N m^{-3} day^{-1}) in the high resolution simulations. Left: low grazing, right: high grazing. Isotherms are also indicated.

compensate from sedimentation of detritus, which sink at 5 m day^{-1}. With respect to the effect of grazing on export of organic matter, there are observational evidences showing that some zooplankton (called flux feeders) feed on settling detritus, which tends to enhance recycling (Gonzales and Smetacek, 1994; Kiorboe, 1997).

4.3. Mean vertical profiles of biomass in low resolution (LR) versus high resolution (HR) simulations

Figs. 11 and 12 give us some further insights on the effect of fine scale dynamics and grazing on the vertical distribution of biological fields. Fig. 11 shows the mean vertical profiles of each biological field at the equilibrium in the four simulations depending on resolution and grazing pressure. In the Low resolution–Low Grazing simulation (Fig. 11a), the model reaches a stationary steady state which is characterized by a nearly complete competitive exclusion of phytoplankton P_1, except in the surface layer where it slightly emerges. This equilibrium is typical of an oligotrophic environment with a nutricline located close to 100 m, and a typical subsurface maximum of phytoplankton (P_2) and detritus (D). We notice here that such equilibrium with subsurface chlorophyll maximum is reached because of sinking detritus and remineralization mechanism (Hodges and Rudnick, 2004). Here the nutricline is situated above the initial euphotic depth (150 m) which can be thought as close to the euphotic depth defined with the 0.1% criterion. In fact the nutricline depth is situated in between the 1% and 0.1% criterion euphotic depth, as it is usually observed in oligotrophic regions. In the Low Resolution–High Grazing simulation (Fig. 11c) the model also reaches a stationary steady state. However, in comparison with the Low Grazing simulation, the ecosystem structure has shifted from a nearly competitive exclusion of P_1 to coexistence between P_1 and P_2. P_1 significantly emerges in the surface layers with a maximum at the base of the mixed layer, while P_2 still dominates below in the subsurface maximum. The zooplankton plays a key role in preventing P_2 from developing through its grazing pressure which is more pronounced on this faster growing phytoplankton.

In the High Resolution–Low Grazing simulation (Fig. 11b), the fine scale variability induces a nutrient pumping from the aphotic zone which stimulates the ecosystem response, in accordance with previous studies (Spall and Richards, 2000; Lévy et al., 2001). As a consequence of vertical velocities generated by mesoscale dynamics which push the pycnocline and the nutricline upward, the depth of the subsurface maximum becomes shallower within the mesoscale region (close to 60 m) and its vertical extension is increased. In the High Resolution–High Grazing simulation (Fig. 11d), the results on average are close to the Low Grazing–High Resolution simulation, except that the biomass of P_2 is considerably reduced. In this case P_2 concentration is close to P_1 because of the grazing pressure. The subsurface maximum of P_1 is shifted upward.

4.4. Zonal mean cross section

The zonal mean cross sections in the high resolution simulations are presented in Fig. 12. In the mesoscale region the nutricline is pushed upward. We have verified that this part of the domain is characterized by a mean vertical input of nutrients from below (not shown). This nutrient input induces an increase of nutrient uptake in the surface layers, and then downwellings associated to mesoscale structures in this region bring poor waters downward. As a consequence, the mean nutrient concentration in this region is lower than surrounding waters at depth down to more than 200 m. In the low grazing model we observe a marked asymmetry between north and south in the mean phytoplankton biomass distribution. P_1 develops mainly in the filamentary region from surface down to 60–100 m, while P_2 develops preferentially in the northern part of the domain, at the base of the nutricline. In the high grazing model, the vertical distributions of both phytoplanktons are more close and symmetric. Let us look now at the biological fluxes. The primary production is strongly correlated with biomass (not shown). The maximum of export is situated south of the front, in the filamentary region, in subsurface centred at 800 km in the meridional direction. When grazing pressure is low we observe a northward extension of this maximum. The maximum of export is well correlated with the maximum of P_2 biomass. This region situated in the filamentary region is characterized by a mean vertical export of nutrients.

5. Conclusion

Results of a model of realistic mesoscale turbulence of a frontal region in the ACC have been presented to study the effects of mesoscale and submesoscale dynamics on the plankton ecosystems structure. In our modeling approach two phytoplankton size classes compete for light and nutrients. The parameterization of phytoplankton competitiveness used in this study is based on Banse (1992) and

Margalef (1979). A particular attention was given to the role of grazing.

The analysis of spatial distribution of biomass reveals that the mesoscale and sub-mesoscale processes strongly constrain the ecosystem structure, creating a spatial segregation between the two phytoplankton size classes. Outside the central frontal region the dominance of large phytoplankton is strongly favoured into nutrient rich fine scale filaments. In this filamentary region, with low grazing pressure, we observe a significant anti-correlation between the two phytoplankton classes, nevertheless the large phytoplankton dominates everywhere. With high grazing pressure the spatial correlation between the two phytoplankton classes becomes positive, but the dominance of large phytoplankton is reduced in high nutrients filaments whereas the dominance of P_1 is increased outside. This spatial segregation is mainly observed in the southern part of the front where filamentary dynamics is particularly active. Inside the central frontal region (mesoscale region) the ecosystem dynamics is different. Whatever the grazing pressure is, the biomasses of the two phytoplankton classes are strongly correlated and localized close to downwelling regions whereas nutrient-rich regions are localized close to upwelling regions.

A statistical analysis of the effects of fine scale dynamics and grazing shows that for the different grazing pressures the fine scale dynamics globally increases the large phytoplankton competitiveness in surface layers and decreases it in subsurface. The effect of grazing is very sensitive to fine scale dynamics. Without fine scale dynamics this effect is weak and tends to decrease the competitiveness of the dominant species depending on depth (small phytoplankton in surface layers and large phytoplankton in subsurface). With fine scales dynamics the effect of grazing is much more significant: in surface layers it induces a shift in phytoplankton dominance from large to small phytoplankton, whereas the dominance of large phytoplankton is maintained below the mixed layer.

It is also shown that fine scales dynamics has a strong impact on both primary and export production. However it is also shown that these effects strongly depend on the grazing pressure. With low grazing pressure, taking into account fine scales dynamics increases both primary and export production. On the contrary, with high grazing pressure, primary production still increases whereas export production decreases.

These results have shown that the effects of small-scales dynamics on the competition between P_1 and P_2 are very sensitive to the grazing parameterization. In our study this grazing pressure is induced by a very simplified parameterization including only one "generic" zooplankton class, in-between micro- and mesozooplankton, with the same preference for each phytoplankton and detritus. This parameterization is somewhat crude, and a better understanding of the ecosystem response to small-scales dynamics requires a finer description of the zooplankton trophic level. Especially an attention has to be given to the functional diversity of these organisms, how do they feed (swimming, catching food) and what is their role in controlling phytoplankton community structure and nutrients dynamics (Franks, 2001). Concerning nutrients, the phytoplankton growth limitation by different elements is important, in particular silicates for diatoms, but also iron in the Southern Ocean. The frontal dynamics playing the role of nutrient injector into the euphotic zone may play a crucial role in these co-limitations and thus on the structure of the planktonic ecosystem. These questions are left to further investigations.

Acknowledgements

We thank Patrice Klein and Peter Franks and three reviewers for many helpful comments. Simulations were performed on the NEC-SX5 of the IDRIS Centre. This work was funded by the CNRS through the PROOF programme. This is the contribution no. 997 of the IUEM, European Institute for Marine Studies (Brest, France).

References

Abraham, E.R., 1998. The generation of plankton patchiness by turbulent stirring. Nature 39, 577–580.

Backus, R.H. (Ed.), 1987. Georges Bank. MIT Press, Cambridge, MA. 593 pp.

Banse, K., 1992. Grazing, temporal changes of phytoplankton concentrations, and the microbial loop in the open sea. In: Falkowski, P.G., Wood, A.D. (Eds.), Primary Productivity and Biogeochemical Cycles in the Sea. Plenum Press, New York, pp. 409–440.

Blanke, G., Delecluse, P., 1993. Variability of the tropical Atlantic Ocean simulated by a general circulation model with two mixed-layer physics. Journal of Physical Oceanography 23, 1363–1388.

Blasco, D., Packard, T.T., Garfield, P.C., 1982. Size dependance of growth rate, respiratory electron transport system activity and chemical composition of marine diatoms in the laboratory. Journal of Phycology 18, 58.

Boyd, P.W., Law, C.S., 2001. The Southern Ocean Iron RElease Experiment (SOIREE): introduction and summary. DSR II 48, 2425–2738.

Claustre, H., Kerhervé, P., Marty, J.-C., Prieur, L., Videau, C., Hecq, J.-H., 1994. Phytoplankton dynamics associated with a geostrophic

front: ecological and biogeochemical implications. Journal of Marine Research 52, 711–742.
Dadou, I., Garcon, V., Andersen, V., Flierl, G.R., Davis, C.S., 1996. Impact of the North Equatorial Current meandering on a pelagic system: a modeling approach. Journal of Marine Research 54, 311–342.
Davis, C.S., 1984. Predatory control of copepod seasonal cycles on Georges Bank. Marine Biology 82, 31–40.
Davis, C.S., 1987. Zooplankton life cycles. In: Backus, R.H. (Ed.), Georges Bank. MIT Press, Cambridge, MA, pp. 256–267.
Falkowski, P.G., Ziemann, D., Kolber, Z., Bienfang, P.K., 1991a. Nutrient pumping and phytoplankton response in a subtropical mesoscale eddy. Nature 352, 544–551.
Falkowski, P.G., Ziemann, D., Kolber, Z., Bienfang, P.K., 1991b. Role of eddy pumping in enhancing primary production in the ocean. Nature 352, 55–58.
Fasham, M.J.R., Ducklow, H.W., McKelvie, S.M., 1990. A nitrogen-based model of plankton dynamics in the oceanic mixed layer. Journal of Marine Research 48, 591–639.
Flierl, G.R., Davis, C.S., 1993. Biological effects of Gulf Stream meandering. Journal of Marine Research 51/3, 529–560.
Foujols, M.-A., Lévy, M., Aumont, O., Madec, G., 2000. OPA 8.1 Tracer Model reference Manual. Note technique du pôle de modélisation, Institut Pierre Simon Laplace, IPSL. http://www.lodyc.jussieu.fr/opa/.
Franks, P.J.S., 2001. Phytoplankton blooms in a fluctuating, environment: the roles of plankton response time scales and grazing. Journal of Plankton Research 23/12, 1433–1441.
Franks, P.J.S., Walstad, L.J., 1997. Plankton patches at fronts: a model of formation and response to wind events. Journal of Marine Research 55, 1–29.
Gonzales, H.E., Smetacek, V., 1994. The possible role of cyclopoid copepods Oithona in retarding vertical flux of zooplankton faecal material. Marine Ecology. Progress Series 113, 233–246.
Hakim, G.J., Snyder, C., Muraki, D.J., 2002. A new surface model for cyclone–anticyclone asymmetry. Journal of Atmospheric Sciences 59, 2405–2420.
Hense, I., Timmermann, R., Beckmann, A., Bathmann, U.V., 2003. Regional ecosystem dynamics in the ACC: simulations with a three-dimensional ocean–plankton model. Journal of Marine Systems 42 (1&2), 31–51.
Hitchcock, G.L., Mariano, A.J., Rossby, T., 1993. Mesoscale pigment fields in the Gulf Stream: observations in a meander crest and trough. Journal of Geophysical Research 948, 8425–8445.
Hodges, B.A., Rudnick, D.L., 2004. Simple models of steady deep maxima in chlorophyll and biomass. Deep-Sea Research, I 51, 999–1015.
Hood, R.R., Habbott, M.R., Huyer, A., 1991. Phytoplankton and photosynthetic light response in a coastal transition zone off northern California in June 1987. Journal of Geophysical Research 96, 14769–14780.
Hulot, F.D., Lacroix, G., Lesher-Moutoué, F., Loreau, M., 2000. Functional diversity governs ecosystem response to nutrient enrichment. Nature 405, 340–344.
Kana, T.M., Glibert, P.M., 1987. Effect of irradiances up to 2000 μE m^{-2} $s^{-}1$ on marine Synechococcus WH7803: Growth: I. Pigmentation, and cell composition. Deep-Sea Research 34, 479–495.
Karsten, R., Jones, H., Marshall, J., 2002. The role of eddy transfer in setting the stratification and transport of a circumpolar current. Journal of Physical Oceanography 32, 39–54.
Kiorboe, T., 1997. Population regulation and role of mesozooplankton in shaping marine pelagic food webs. Hydrobiologia 363, 13–27.
Klein, P., Treguier, A.-M., Hua, B.L., 1998. Three dimensional stirring of thermohaline fronts. Journal of Marine Research 56, 589–612.
Lévy, M., Klein, P., 2004. Does the low frequency variability of mesoscale dynamics explain a part of the phytoplankton and zooplankton spectral variability? Proceedings of the Royal Society of London 460-2046, 1673–1683.
Lévy, M., Klein, P., Tréguier, A.M., 2001. Impact of sub-mesoscale physics on production and subduction of phytoplankton in an oligotrophic regime. Journal of Marine Research 59, 535–565.
Lima, I.D., Olson, D.B., Doney, S.C., 2002. Biological response of frontal dynamics and mesoscale variability in oligotrophic environments: biological production and community structure. Journal of Geophysical Research 107, 25–46.
Madec, G., Chartier, M., Delecluse, P., Crepon, M., 1991. A three dimensional numerical study of deep water formation in the northwestern Mediterranean Sea. Journal of Physical Oceanography 21, 1349–1371.
Madec, G., Delecluse, P., Imbard, M., Lévy, C., 1999. OPA8.1 Ocean General Circulation Model Reference Manual, Note du Pôle de modélisation, Institut Pierre Simon Laplace. http://www.lodyc.jussieu.fr/opa/.
Mahadevan, A., Archer, D., 2000. Modeling the impact of fronts and mesoscale circulation on the nutrient supply and biogeochemistry of the upper ocean. Journal of Geophysical Research 105, 1209–1225.
Margalef, R., 1979. Life forms of phytoplankton as survival alternatives in an unstable environment. Oceanologica Acta I, 493–509.
Martin, A.P., Srockoz, M.A., 2002. Plankton distribution spectra: inter-size class variability and the relative slopes for phytoplankton and zooplankton. Geophysical Research Letters 29, 2213–2217.
Martin, A.P., Richards, K.J., Fasham, M.J.R., 2001. Phytoplankton production and community structure in an unstable frontal region. Journal of Marine Systems 28, 65–89.
Martin, A.P., Richards, K.J., Bracco, A., Provenzale, A., 2002. Patchy productivity in the open ocean. Global Biogeochemical Cycles 16.
McGillicudy, D.J., Robinson, A.R., 1997. Eddy-induced nutrient supply and new production in Sargasso Sea. Deep-Sea Research, Part I 44, 1427–1450.
Morel, A., 1991. Light and marine photosynthesis: a spectral model with geochemical and climatological implications. Progress in Oceanography 26, 263–306.
Oschlies, A., Garçon, V., 1998. Eddy-induced enhancement of primary production in a model of the North Atlantic Ocean. Nature 394, 266–269.
Rivière, P., Treguier, A.M., Klein, P., 2004. Effects of bottom friction on the nonlinear dynamics of a baroclinic oceanic jet. Journal of Physical Oceanography 34 (2), 416–432.
Rodriguez, J., Tintoré, J., Allen, J.T., Blanco, J.M., Gomis, D., Reul, A., Ruiz, J., Rodriguez, V., Echevarria, F., Jiménez-Gomez, F., 2001. Mesoscale vertical motion and the size structure of phytoplankton in the ocean. Nature 410, 360–363.
Spall, S.A., Richards, K.J., 2000. A numerical model of mesoscale frontal instabilities and plankton dynamics: I. Model formulation and initial experiments. Deep-Sea Research, Part I 47, 1261–1301.
Strass, V.H., Naveira Garabato, A.C., Pollard, R.T., Fischer, H.I., Hense, I., Allen, J.T., Read, J.F., Leach, H., Smetacek, V., 2002. Mesoscale Frontal Dynamics: shaping the environment of primary production in the Antarctic Circumpolar Current. Deep-Sea Research 49/18, 3735–3769.